Supporting Information

Large-area in-Situ Growth of Flexible Perovskite scintillator Film for X-ray indirect detection applications

Hongyu Lv, [a,b] Qun Hao,[a,c] Naiquan Yan,[a] Lisha Ma,[a] and Menglu Chen,*[a,b,c]

a School of Optics and Photonics, Beijing Institute of Technology, Beijing 100081, China;
b Westlake Institute for Optoelectronics, Fuyang, Hangzhou 311421, China
c Physics department, Changchun Institute of Technology, Changchun, 130003, China
* *Corresponding author: menglu@bit.edu.cn*

This PDF file includes:

Supporting Figures

The preparation process schematic diagram of $CsPbBr_3$@VmB1@PMMA film, as shown in Fig. S1. The 0.6 mmol of CsBr, 0.4 mmol of $PbBr_2$ and *x* mmol VmB1 (*x*=0, 0.02, 0.04, 0.06, and 0.08) powders are added to 5 mL DMF, respectively. The precursor solution is heated and stirred until the powders are completely dissolved. Then, the 900 μL precursor solution is added to 5 mL PMMA/DMF solution. Next, the mixed solution is spin coated in quartz glass and annealing in high temperature.

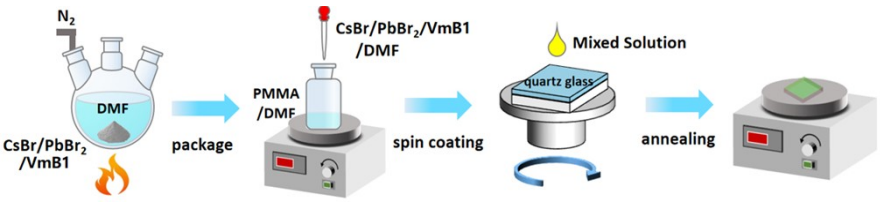

Fig. S1. Schematic diagram of the synthesize of $CsPbBr_3$@VmB1@PMMA film.

In Fig. S2(a-f), it can be clear seen that the $CsPbBr_3$ NCs began to in-situ grow rapidly until 90 s after annealing, and the NCs covered the substrate to form a uniform film. Due to the non-uniform nucleation growth mode of $CsPbBr_3$ NCs in PMMA/DMF solution, their growth positions are randomly distributed.

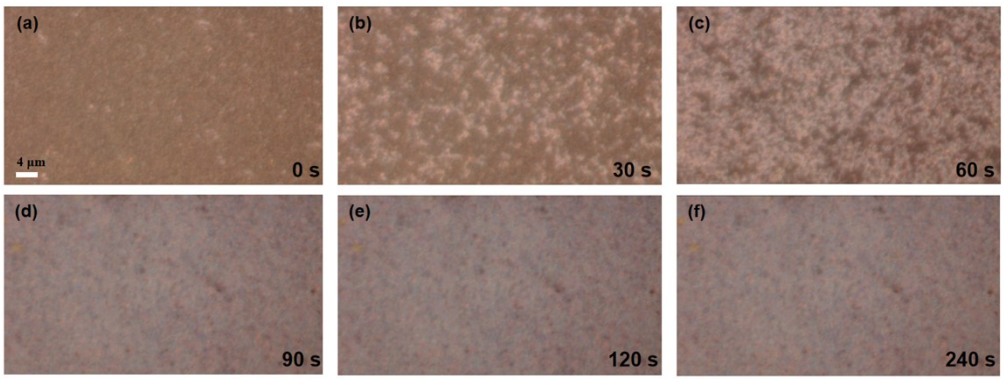

Fig. S2(a-f). The microscopic images of the $CsPbBr_3$@VmB1@PMMA film after annealing at 90 °C for different time.

As shown in Fig. S3, the C 1s and O1s of signals are all from the PMMA matrix on the surface of the perovskite film.

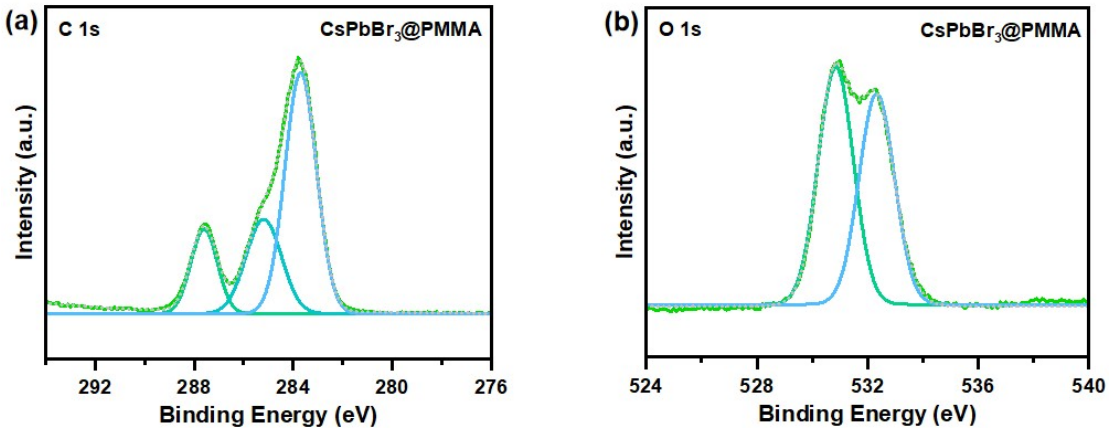

Fig. S3(a-b). XPS spectra of $CsPbBr_3$@PMMA film for C 1s and O 1s.

In Fig. S4, we use NaCl/water solution (30mg/mL) to simulate seawater. The results show that the $CsPbBr_3$@VmB1@PMMA film has good stability in simulated seawater solution, and the luminous intensity of $CsPbBr_3$@VmB1@PMMA film can be maintained at 94.1 % of the initial luminous intensity in simulated seawater solution for 480 hours.

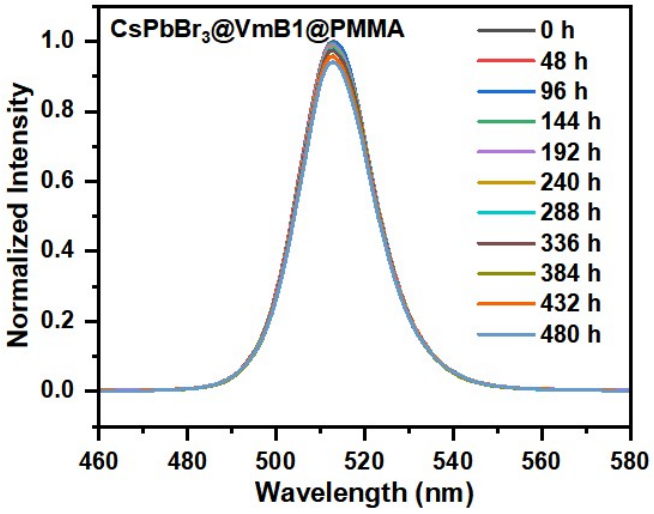

Fig. S4. The stability of $CsPbBr_3$@VmB1@PMMA film in salt solution.

As depicted in Fig. S5(a-b), it can be observed that the $CsPbBr_3$@VmB1@PMMA film still shows bright green luminescence after being immersed in the NaCl/water solution for 480 hours.

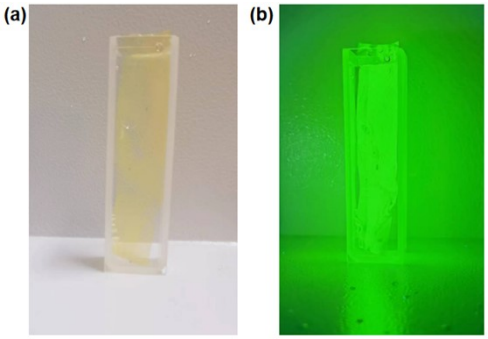

Fig. S5(a-b). Photograph of $CsPbBr_3$@VmB1@PMMA film immersed in simulated seawater solution for 10 days under (a) sunlight and (b) 365 nm ultraviolet lamp irradiation, respectively.

As shown in Fig. S6, the $CsPbBr_3$@VmB1@PMMA film exhibit high water stability, its luminous intensity can be maintained at 96.5 % of the initial luminous intensity in the water for 480 hours.

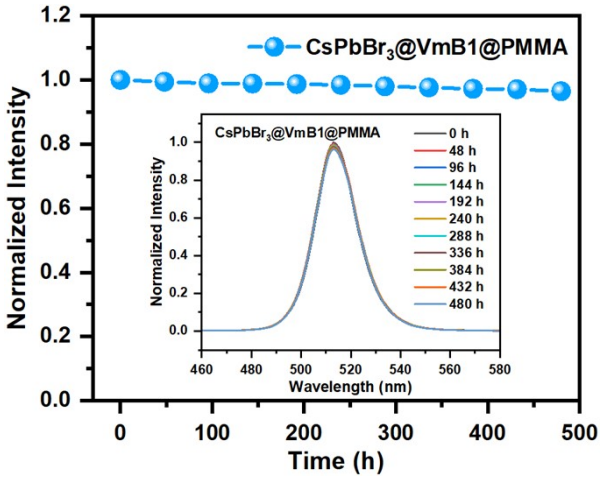

Fig. S6. Normalized spectra and dot plot (inset) of the water stability of $CsPbBr_3$@VmB1@PMMA film.

Fig. S7(a-b) shows the $CsPbBr_3$@VmB1@PMMA film still shows bright green luminescence after being immersed in the water for 480 hours.

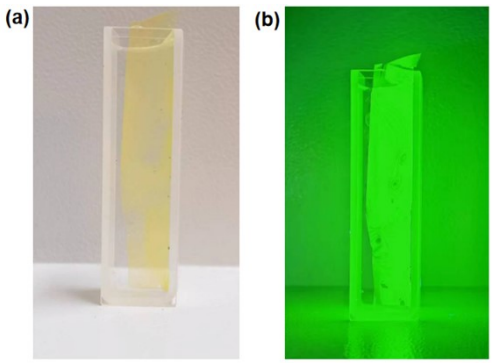

Fig. S7. Photograph of $CsPbBr_3$@VmB1@PMMA film immersed in water for 480 hours under (a) sunlight and (b) 365 nm ultraviolet lamp irradiation, respectively.

In order to verify that the $CsPbBr_3$@PMMA@VmB1 film can long-term use in a deep-sea high-pressure environment, we observed the photos of the film under different pressures, as shown in Fig. S8. The results show that the film still exhibit bright green luminescence under 20 Mpa pressure, which pressure is about the pressure at 2040 meters under the deep-sea.

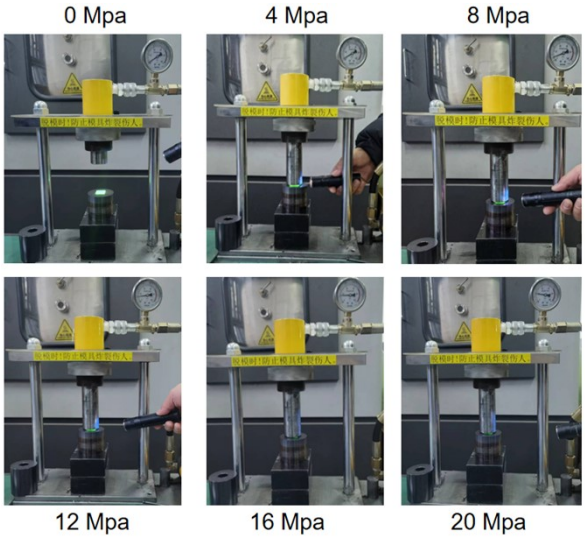

Fig. S8. Photographs of the $CsPbBr_3$@PMMA@VmB1 film under different pressures.

Fig. S9 show that the thickness of the film did not change significantly, and the flatness is improved under high pressure environment.

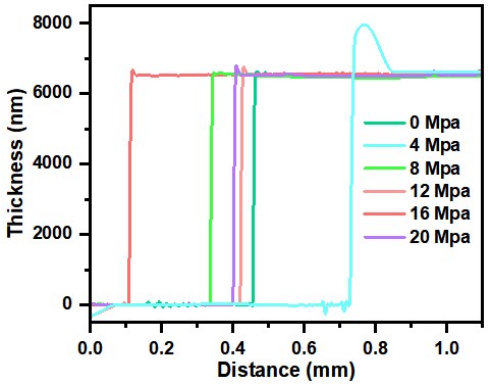

Fig. S9. The step profiler measurement of $CsPbBr_3$@PMMA@VmB1 film under different pressures.

As shown in Fig. S10, the emission intensity of $CsPbBr_3$@PMMA@VmB1 film at 90 ℃ remains 34% of initial intensity at room temperature.

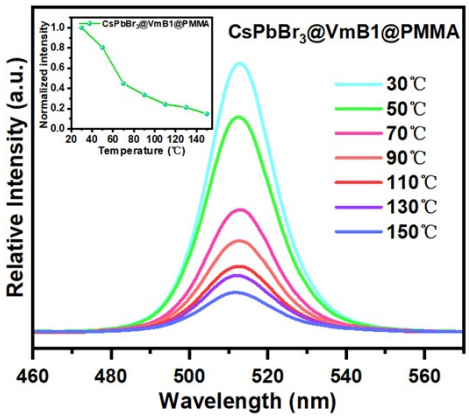

Fig. S10. Temperature-dependent PL spectra of $CsPbBr_3$@PMMA@VmB1 film under 365 nm ultraviolet irradiation.

The measurement for stability of the $CsPbBr_3$@VmB1@PMMA film in the sulfur-rich environment is shown in Fig. S11(a-b). We heat the $(NH_4)_2S$ solution to generate SO_2 to create a S-rich environment. It can be clear observed that the color of the allochroic silica gel is changed from blue to black, which confirms that a large amount of SO_2 gas is generated in the flask.

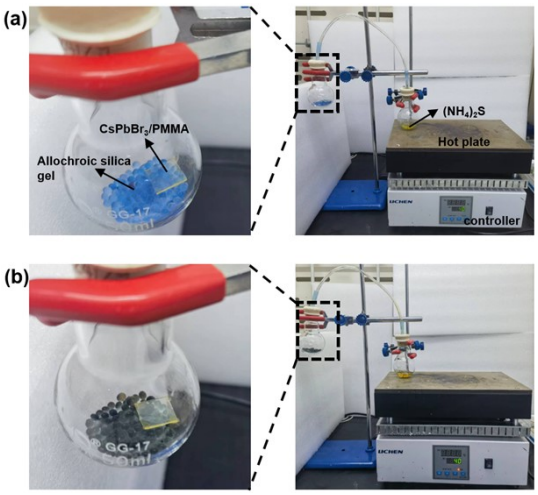

Fig. S11(a-b). Device diagram of $CsPbBr_3$@VmB1@PMMA film before and after fumigation in sulfur-rich environment.

As shown in Fig. S12, the $CsPbBr_3$@VmB1@PMMA film can maintain 86.5% of initial intensity in a sulfur-rich environment for 10 hours.

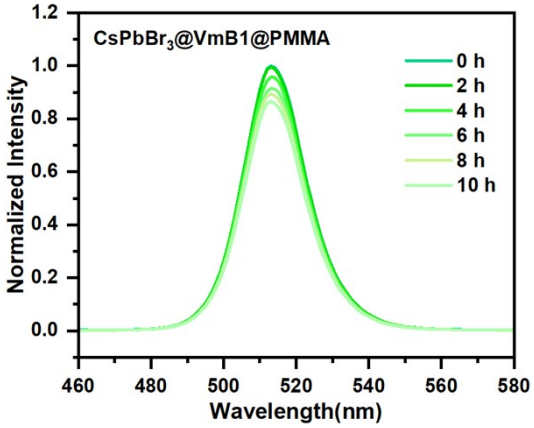

Fig. S12. Under 365 nm UV lamp irradiation, the PL spectra of $CsPbBr_3$@VmB1@PMMA film in sulfur-rich environment with different time.

In Fig. S13, $CsPbBr_3$ NCs is a typical octahedral unit cell.

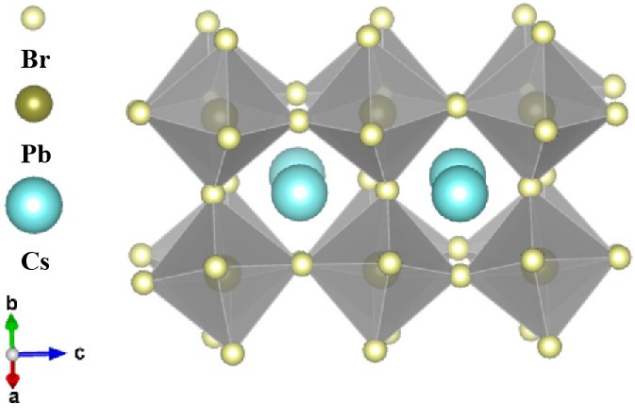

Fig. S13. Crystal structure of $CsPbBr_3$ NCs.

As shown in Fig. S14, the absorption and luminescence properties of the $CsPbBr_3$@PMMA film is optimized when the ratio of $CsBr/PbBr_2$ is 3:2.

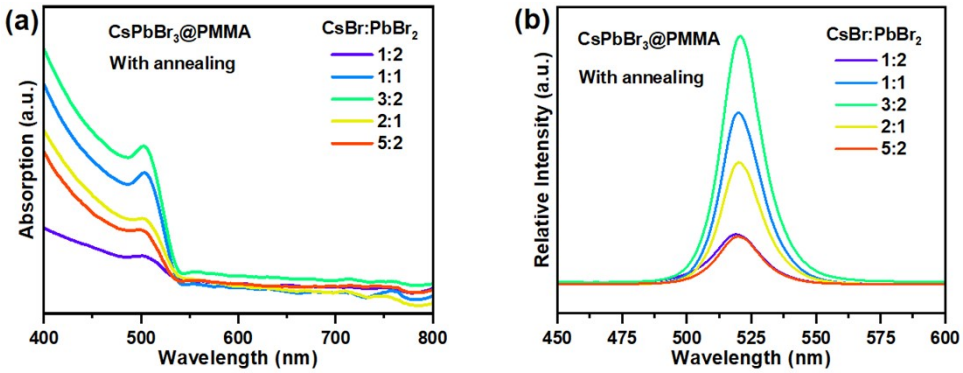

Fig. S14(a-b). The absorption and PL spectra of $CsPbBr_3$@PMMA film synthesized at different $CsBr/PbBr_2$ ratios.

With the increase of VmB1 doping concentration, the luminescence color of the $CsPbBr_3$@*x*VmB1@PMMA film (*x*=0, 0.05, 0.1, 0.15, and 0.2) show slight changes, but they are still exhibited green emission in Fig. S15.

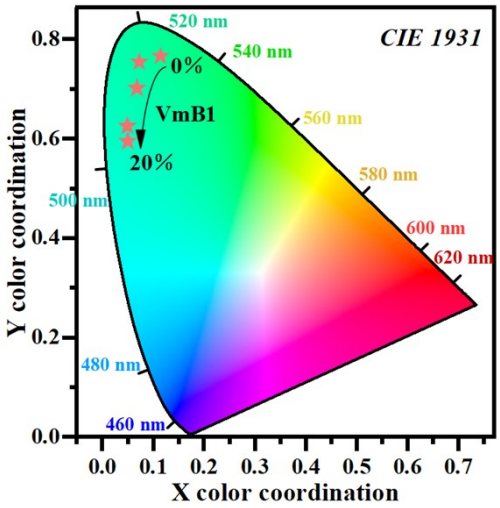

Fig. S15. CIE coordinates of $CsPbBr_3$@*x*VmB1@PMMA (*x*= 0, 0.05, 0.1, and 0.2) film.

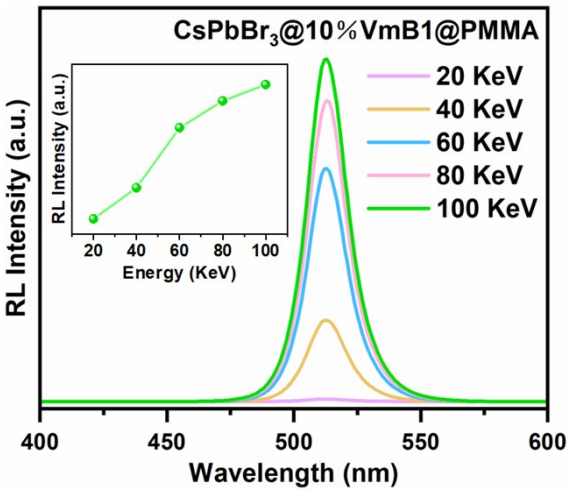

Fig. S16. RL spectra of $CsPbBr_3$@10%VmB1@PMMA film at different X-ray energies.

The fitted time-related RL decay results of $CsPbBr_3$@10%VmB1@PMMA film are showed in Fig. S17. The average lifetime (τ_{ave}) is obtained by the equation of $\tau_{ave} = (A_1\tau_1^2 + A_2\tau_2^2 + A_3\tau_3^2) / (A_1\tau_1 + A_2\tau_2 + A_3\tau_3)$.

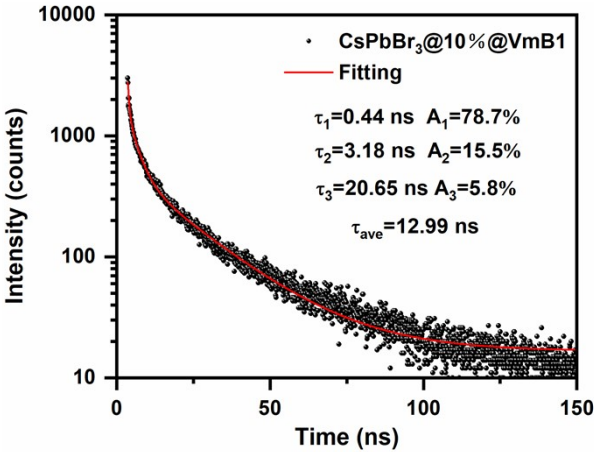

Fig. S17. RL decay profile of $CsPbBr_3$@10%VmB1@PMMA film.

In Fig. S18(a-b), it can be seen that the 10 μm perovskite film has the best imaging resolution. When the film thickness is less than 10 μm, the film may not fully absorb X-ray. With the increase of film thickness from 10 to 50 μm, the X-ray imaging quality reduce, which is attributed to the enhanced X-ray scattering effect for thicker films.[1]

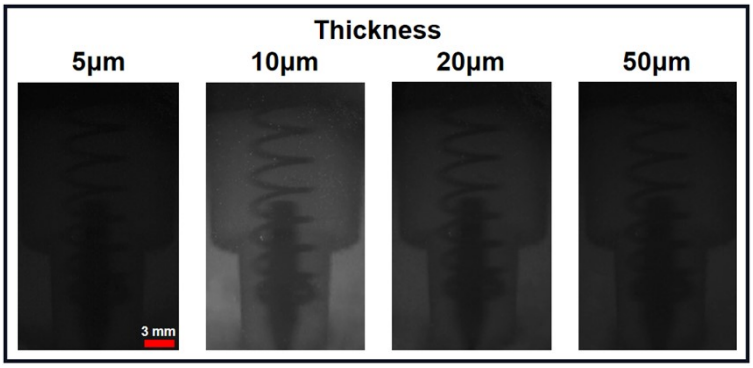

Fig. S18(a-b). The images of a ballpoint pen tip under different thickness (5, 10, 20, 50 μm) of $CsPbBr_3$@VmB1@PMMA films.

By covering the film on the substrate of the detector, the interdigitated electrodes with different areas in the middle can be observed, which indicates that the $CsPbBr_3$@VmB1@PMMA film has good transparency, as shown in Fig. S19(a-b).

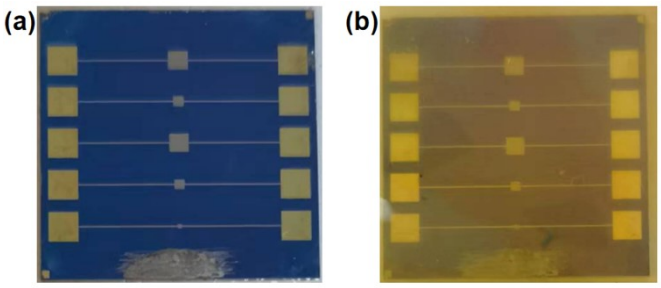

Fig. S19(a-b). Transparency test of $CsPbBr_3$@VmB1@PMMA film.

In Fig. S20, an as-prepared X-rays photodetection is combined with $CsPbBr_3$@VmB1@PMMA film and silicon detector, the optical signal emitted by the film is read

out by the back-end silicon detector in the form of an electrical signal under the stimulation of the excitation light source.

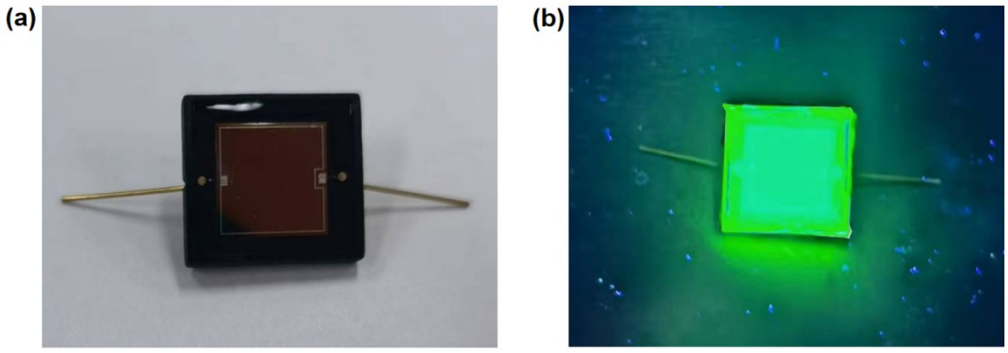

Fig. S20(a-b). Photographs of the coupling of $CsPbBr_3$@VmB1@PMMA film and the silicon detector under (a) daylight and (b) ultraviolet light.

Supporting Tables

Table S1. The fitted time-related PL decay results of $CsPbBr_3$@*x*VmB1@PMMA film (*x*=0, 0.05, 0.1, 0.15, and 0.2). The average lifetime (τ_{av}) is obtained by the equation of $\tau_{av} = (A_1\tau_1^2 + A_2\tau_2^2) / (A_1\tau_1 + A_2\tau_2)$.

Sample	A_1	τ_1 (ns)	A_2	τ_2 (ns)	τ_{av} (ns)	χ^2
$CsPbBr_3$	**0.20**	**4.81**	**0.80**	**18.87**	**7.61**	**0.999**
$CsPbBr_3$@5%VmB1	**0.16**	**4.96**	**0.84**	**25.40**	**10.34**	**0.999**
$CsPbBr_3$@10%VmB1	**0.15**	**5.68**	**0.85**	**33.05**	**15.66**	**0.998**
$CsPbBr_3$@15%VmB1	**0.14**	**5.18**	**0.86**	**31.25**	**13.40**	**0.997**
$CsPbBr_3$@20%VmB1	**0.16**	**3.48**	**0.84**	**18.91**	**6.56**	**0.997**

References

[1] Q. S. Chen, J. Wu, X. Y. Ou, B. L. Huang, J. Almutlaq, A. A. Zhumekenov, X. W. Guan, S. Y. Han, L. L. Liang, Z. G. Yi, J. Li, X. J. Xie, Y. Wang, Y. Li, D. Y. Fan, D. B. L. Teh, A. H. All, O. F. Mohammed, O. M. Bakr, T. Wu, M. Bettinelli, H. H. Yang, W. Huang, X. G. Liu, *Nature*, 2018, **561**, 88.